Electrochemistry of Praseodymium in Aqueous Solution Using a Liquid Gallium Cathode

To cite this article before publication: Eugene Engmann *et al* 2022 *J. Electrochem. Soc.* in press https://doi.org/10.1149/1945-7111/ac76e3

Electrochemistry of Praseodymium in Aqueous Solution Using a Liquid Gallium Cathode

Journal:	*Journal of The Electrochemical Society*
Manuscript ID	JES-107427.R1
Manuscript Type:	Research Paper
Date Submitted by the Author:	19-May-2022
Complete List of Authors:	Engmann, Eugene; Idaho National Laboratory, Chemical Separations Diaz Aldana, Luis; Idaho National Laboratory, Lister, Tedd; Idaho National Laboratory Research Library, Chemical Separations Palasyuk, Olena; Ames Laboratory Zhao, Haiyan; University of Idaho, Chemical and Materials Engineering
Keywords:	Rare earth element, gallium, Electrodeposition, Alloy formation

Electrochemistry of Praseodymium in Aqueous Solution Using a Liquid Gallium Cathode

Eugene Engmann,[1,2] Luis A. Diaz,[1] Tedd E. Lister,[1,z] Olena Palasyuk,[3] and Haiyan Zhao[4]

[1]Critical Materials Institute, Idaho National Laboratory, Idaho Falls, Idaho 83402, United States

[2]University of Idaho, Department of Nuclear Engineering and Industrial Management, Iowa, United States
[3]Ames Laboratory, Department of Energy U.S., Critical Materials Institute, Ames, Iowa 50011-3020, United States

[4]University of Idaho, Department of Chemical and Biological Engineering, Idaho Falls, Idaho 83404, United States

[z]E-mail: Tedd.lister@inl.gov

Abstract

The electrochemistry of liquid Ga electrodes in aqueous media was examined in the presence of praseodymium acetate (PrOAc) as an alternate path for low temperature reduction of rare earth elements (REE). This study investigated the aqueous electrochemistry of Ga with and without REEs (Pr). Cyclic voltammetry experiments showed that in the presence of PrOAc, an order of magnitude increase in cathodic current was observed for the Ga electrode, compared to that in the absence of Pr. Decrease in the reduction current with the increase of scan rate, with and without Pr, suggests catalytic reactions following electron transfer, which was attributed to the Ga_2O disproportionation reaction. Chronoamperometric experiments performed in Pr containing solutions formed a precipitate. Over 50% of the Pr ions from the aqueous electrolyte were immobilized in the precipitate; a solid Ga-rich phase. Formation of this precipitate was only possible when Ga oxidation was induced. This condition was achieved by circulation of liquid Ga from the pool via external pump and returned dropwise to the liquid Ga pool. When the collected precipitate was leached in dilute HCl, Pr was released with H_2 evolved as a byproduct, and Ga returned to its initial liquid metallic state. These preliminary results show encouraging new routes that could be applied for the recovery of diluted REE leachates, such as those obtained from magnets, coal fly ash, and ores.

Introduction

The electrochemical reduction of reactive metals, such as rare earth elements (REEs) is hindered in aqueous media due to extremely negative reduction potentials. This setback occurs due to the limited electrochemical window of water favoring the evolution of hydrogen over metal reduction (1). However, through alloy formation, the chlor-alkali industry has shown that reactive metals such as sodium can be

reduced to the metallic state in aqueous media (2, 3). Hence, the use of amalgam formation (employing mercury) for the processing of REEs was prevalent during the 1940-60s (4-8).

Previously, mercury (Hg) has been employed as electrode material for REE alloy formation, offering a high hydrogen evolution overpotential and an increase in the cathodic potential operating range (6, 9). However, the toxicity of Hg makes its handling and disposal hazardous, expensive, and highly regulated (10, 11). These concerns suggest the need of a material substitute with similar characteristics as Hg, but of a nontoxic nature.

Ga and Ga alloys are possible substitutes for Hg electrodes, due to low melting points. Like Hg, Ga possesses a high hydrogen overpotential without compromising electrochemical behavior and offers surface renewability. Ga is non-toxic and has a lower vapor pressure than Hg. However, it also features more negative reduction potential than Hg (11), which makes Ga and its associated oxide formation less stable than Hg.

The electrochemical nature and complexity of Ga has garnered interest among researchers due to the characteristic of easily forming surface oxide layers (12). Formation of the oxide layer on liquid Ga occurs spontaneously in aqueous solution (13). In aqueous media, Ga exists as various species with β-Ga_2O_3) as its most stable phase. Trivalent speciation for Ga in aqueous solution is pH dependent and may exist as Ga^{3+}, $Ga(OH)^{2+}$, GaO^{+}, GaO_2^{-}, $HGaO_3^{2-}$, or GaO_3^{3-}(14). Flamini *et al.* observed that at low current densities, Ga(III) can be reduced to Ga(I)(15). Recently, Monnens *et al.* showed evidence of the formation of Ga(I) as an intermediate in the reduction of Ga(III) to Ga metal(16). The presence of Ga(I) in the form of Ga_2O was also reported by Hong et al. (17). Other studies have reported that Ga_2O undergoes a disproportionation reaction, , to form Ga metal and Ga(III) due to its instability in aqueous environments (17, 18).

Furthermore, the ability of Ga to dissolve a host of other metals creates a pathway to produce metal and metal oxides (18-20). Mayyas et al. (21)observed that the application of a potential range to GaSn, GaIn and GaZn alloys led to the capture and release of Sn, In and Zn. Other studies have also employed the use of Ga to induce mass transport of target elements by converting the effect of an electrical current into mechanical flow (22-25).

In this work, a deeper understanding of Ga electrochemistry in the presence of a REE specie was driven by interest in using Ga as a medium to reduce and capture REEs directly from aqueous media. This paper reports on the behavior of Ga in lithium acetate (LiOAc) solutions with and without Pr, where oxides play a role in the formation of products at the cathode. LiOAc was selected due to solubility of REEs at higher pH values.

Experimental

Electrochemical experiments

The working electrode was a liquid Ga (99.99%, Rotometals) pool (approximate surface area of 8.04 cm^2) with a Pt wire as current collector. The area of the Pt wire exposed to solution was coated with Teflon. Measurements were performed at 30 °C to maintain Ga as a liquid. The auxiliary electrode was either Pt or IrO_2/titanium mesh for cyclic voltammetry (CV) and bulk electrolysis (BE), respectively. The IrO_2 coating was applied to both sides of a titanium mesh by airbrushing H_2IrO_3 diluted in isopropyl alcohol onto the exposed surfaces followed by heating at 550 °C for 2 h to form IrO_2. Potentials were measured

and reported versus an Ag/AgCl (3 M NaCl) (BASi) reference electrode. Analytical grade lithium acetate (LiOAc) and praseodymium acetate (PrOAc) hydrate 99.9%, were used for electrolyte preparations in deionized water (DI) (>18 MΩ). Chronoamperometry and potentiodynamic experiments were performed using a BioLogic SP-50 potentiostat controlled by EC-Lab software. IR compensation was applied to CV curves. CV experiments were conducted in a single cell as shown in Figure 1a. Bulk electrolysis experiments were conducted in a H-cell depicted in Figure 1b. All experiments were conducted in an open atmosphere environment.

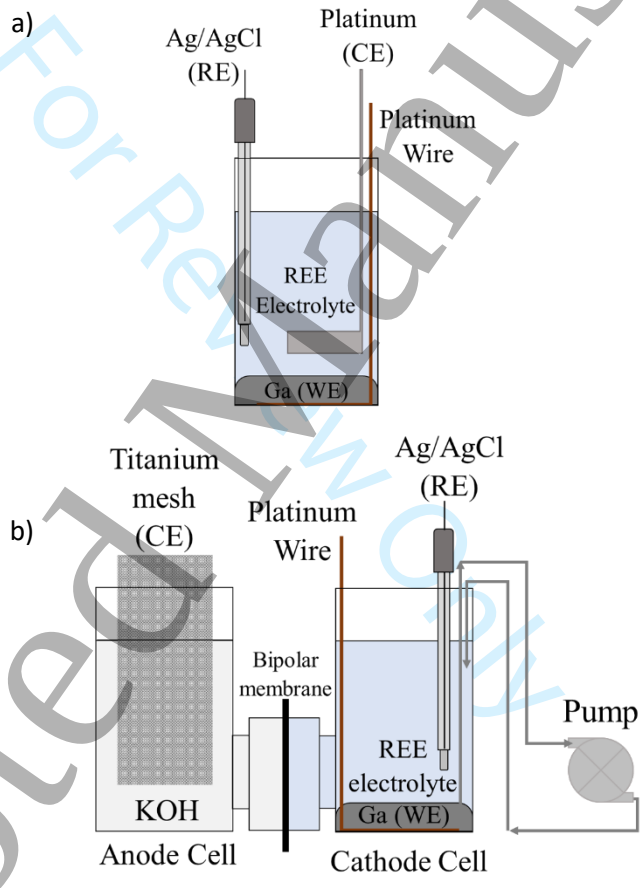

Figure 1. a) Single compartment setup for CV experiments, b) H-cell setup for bulk electrolysis experiments (BE). Lines with arrows represent the circulation of Ga.

Analysis and characterization methods

Following electrochemical tests in PrOAc electrolyte, the liquid Ga was separated from the electrolyte, washed with DI water, and stripped in 1 M HCl. For experiments involving formation of a gray precipitate as a product, the electrolyte was centrifuged, and vacuum filtered to recover the precipitate. For analysis, the precipitate was digested in a 3:1 HCl-HNO_3 or 1 M HCl. The elements Pr and Ga were measured using an iCAP Q inductively coupled plasma mass spectrometer (ICP-MS) from Thermo

Scientific. Peak analysis, and calculation of charge for reduction and oxidation features on CV plots was conducted using an EC-Lab V.11.33 by BioLogic Instruments. EC-Lab integration function was employed without background subtraction, for calculating the charge. SEM and EDS analysis were conducted in a JEOL JSM-6610LV and EDAX AMETEK Apollo X controlled by EDAX software, to study surface morphology, elemental composition, and elemental distribution. SEM and EDS samples were prepared by appropriately placing double sided carbon tape unto sample holders and dipping the opposite side of tape in the dried precipitate product. XRD analysis was conducted to determine the crystallinity of the gray precipitate using a PANalytical X-Pert Pro Diffraction System (Co Kα radiation, λ = 1.78897 Å). A complete description of ICP-MS and XRD analysis is presented in the supporting information file. Elemental analysis of the precipitate was obtained using a 836 Series Elemental Analyzer using inert gas fusion technique to measure overall oxygen content. The Raman spectra of the precipitate was collected using a Bruker SENTERRA II dispersive micro Raman spectrometer equipped with a confocal microscope (20x) from 50 to 3500 cm−1 at 4 cm−1 resolutions using an excitation wavelength of 532 nm (green laser). Laser power was set at 12 mW, while integration time was limited to 2 seconds and 30 scans were accumulated to improve signal-to-noise ratio. The homogenized powdered samples were first pelletized into circular disks, which were then used for the Raman spectroscopic data collection. The Raman data collected at different locations on the pellets of the samples did not show any noticeable change confirming the homogeneity of the samples.

Results and Discussion

Cyclic voltammetry of background electrolyte (0.15 M LiOAc)

The oxidation of Ga to Ga(III), in aqueous media, is thermodynamically favored given the pH of the electrolyte (~6.9) and the potential window (> -0.9 V), used in this work. This is corroborated by the Pourbaix diagram in Figure S1. Furthermore, the formation of Ga(III) oxyhydroxide as suggested, is in agreement with the work done by Varadharaj and Rao(26). Under these conditions, the Pourbaix diagram for gallium in water (14) suggests:

$$4Ga + 3O_2 + 2H_2O \rightleftharpoons 4GaOOH \quad (1)$$

0.15 M LiOAc background electrolyte was employed for the initial electrochemical studies of liquid Ga electrode. Figure 2 shows the current-potential profiles of liquid Ga electrode in the background electrolyte. During potential sweeps, the cathodic limit, $E_{c,}$ was maintained at -1.27 V while the anodic limit, E_a, was incrementally adjusted from -1 to 0.2 V. The selection of -1.27 V as the E_c prevented excessive hydrogen evolution. A reduction peak C_1 at approximately -1.17 V was observed during the first cycle, starting at an initial open circuit potential (OCP) above -0.85 V. However, C_1 decreases significantly in subsequent scans and eventually becomes nonexistent when E_a remains below -0.9 V as shown in Figure 2a. As the forward scan approached -1.17 V, the surface of the Ga pool changed from dull to a shiny in appearance. This suggests the reduction of surface oxides(15, 20). As the potential scan passed below -1.2 V the current increase can be attributed to the hydrogen evolution reaction (HER)[15]. Shortly after reversing the potential (Figure 2a), peak A^* is observed. Peak A^* can be attributed to reduction of adsorbed hydrogen (H_{ads}). This was verified by varying E_c while maintaining E_a at -1 V (Inset of Figure 2a). When E_c is positive of the HER region, A^* disappears. Tsvetanova et al.(27), offered a similar interpretation while studying the anodic dissolution of Ga in acidic aqueous media. Likewise, Varadharaj and Rao (26) also observed a similar phenomenon while studying Ga films in alkaline media.

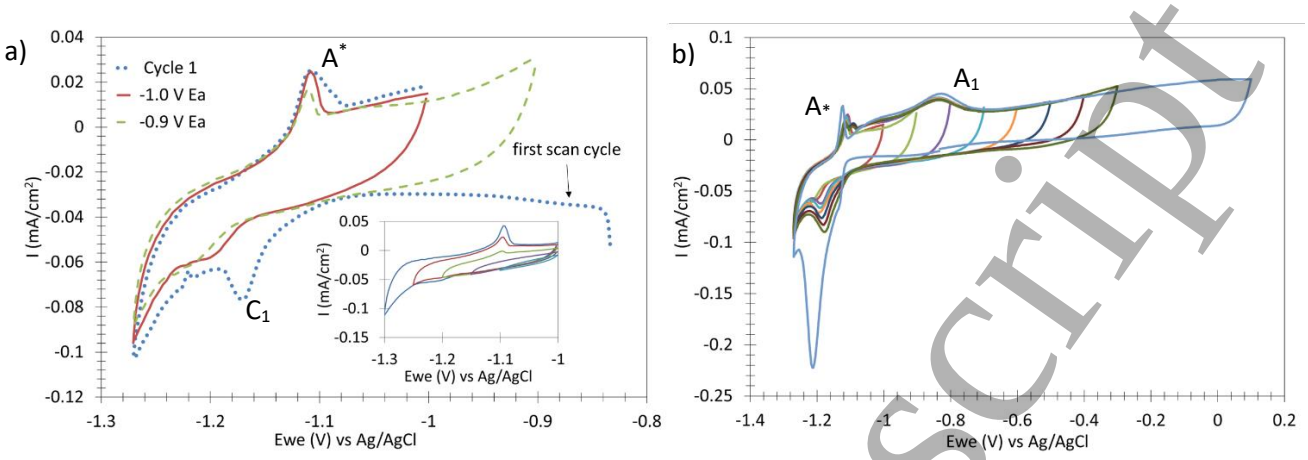

Figure 2. Window opening CV scans of Ga electrode at 10 mV/s in LiOAc (first cycle is blue dashed curve). a) CV scan cycles with cathodic switch potential held at -1.27 and varied from -1.0 V (red solid curve), to -0.9 V (green dash curve) with inset showing response while varying the lower switch potential, b) CV scan cycles where the anode switching potential is varied.

Note that with E_a below -0.9 V, no distinct oxidation peak is observed that can be correlated to C_1. The decrease in the reduction peak C_1 following the first cycle (E_a is below -0.9 V) suggests that C_1 is linked to reduction of the native oxide on Ga. This suggests that in this potential range Ga oxidation is nonexistent or kinetically slow.

Figure 2b shows that increasing E_a to values greater than -0.9 V introduces the broad oxidation wave A_1 (ca. -0.85 V), and the re-appearance of the reduction peak C_1 during the cathodic scan. As E_a increases more positive of -0.8 V, a clear increase in C_1 peak current and peak area was observed. Perkins observed that the appearance of C_1 was influenced by the reduction of oxide products formed at A_1(28). At E_a > -0.8 V A_1 remains unchanged, which could be explained as oxidation of Ga^0 to Ga(I) (Eq-3), an intermediate in the formation of trivalent Ga(III) through a disproportionation reaction. Varadharaj and Rao (26) also attributed the first Ga oxidation peak (A_1) to the formation of Ga_2O.

$$2Ga + H_2O \rightleftharpoons Ga_2O + 2H^+ + 2e^- \quad (2)$$

$$3Ga_2O \rightarrow 4Ga + Ga_2O_3 \quad (3)$$

Following peak A_1 a steady increase in current was observed with increasing potential. Perkins suggested that this increase can be attributed to the continuous formation of Ga_2O_3(29). Hence, increasing formation of Ga_2O_3 is believed to proceed as described in Equations 2 followed by Equation 3.

Ga(III) oxides formed from Equations 1-3 can be electrochemically reduced to Ga metal as suggested by Equation 4. Proposed mechanisms suggest the intermediate formation of Ga_2O (Equations 2 and 3) during the reduction of Ga_2O_3. The formation of Ga_2O cannot be ignored because the reduction potential for the redox couples Ga^{3+}/Ga^+ and Ga^+/Ga^0 -0.40 V and -0.53 vs SHE, respectively, are relatively close(14, 30). Monnens et al. confirmed the formation of Ga(I) as an intermediate in the formation of Ga^0 (Equations 4-6) (16)with a rotating ring disk electrode (RRDE) collection experiment in non-aqueous electrolytes. During their experiments, an increase in ring current was attributed to the reduction of Ga(I) species formed at the disk and collected at the ring.

$$Ga_2O_3 + 6H^+ + 6e^- \rightarrow 2Ga + 3H_2O \quad (4)$$

$$Ga_2O_3 + 4H^+ + 4e^- \rightarrow Ga_2O + 2H_2O \quad (5)$$

$$Ga_2O + 2H^+ + 2e^- \rightarrow 4Ga + H_2O \quad (6)$$

Flamini *et al.* [15] also observed that at low current densities, Ga(III) is reduced to Ga(I). Also, the presence of Ga(I) is reported by Hong *et al.*(17).

Figure S2 and Table S1 show the integration of the anodic and cathodic sweeps at various E_a values for the Ga electrode in LiOAc electrolyte. No background subtraction was performed in this analysis. The charge of the cathodic sweep has a gradual increase and plateaus when E_a is over -0.2 V. The anodic sweep charge shows a steady increase as E_a approaches more positive values. A tentative explanation of the greater charge values for oxidation could be the partial dissolution of trivalent gallium species into the electrolyte. Accordingly, based on the cathodic peak charge value for peak C_1, the approximate oxide thickness calculated from the reduction peak C_1 is shown in Figure S3. This plot shows a relatively thin oxide layer (<10 nm) forming with E_a negative of 0.2 V and growing steeply at more positive values.

Cyclic voltammetry scan rate study in the absence of Pr

Evaluation of the peak current density (j_P) as a function of the scan rate (v) was performed to better understand the redox mechanisms of Ga. The CV curves acquired in these experiments are provided in Figure S4 where E_a was held at 0.2 V. Figure 3 shows that at lower v a linear relationship of j_p with v and $v^{1/2}$ suggests a diffusion-controlled mechanism.

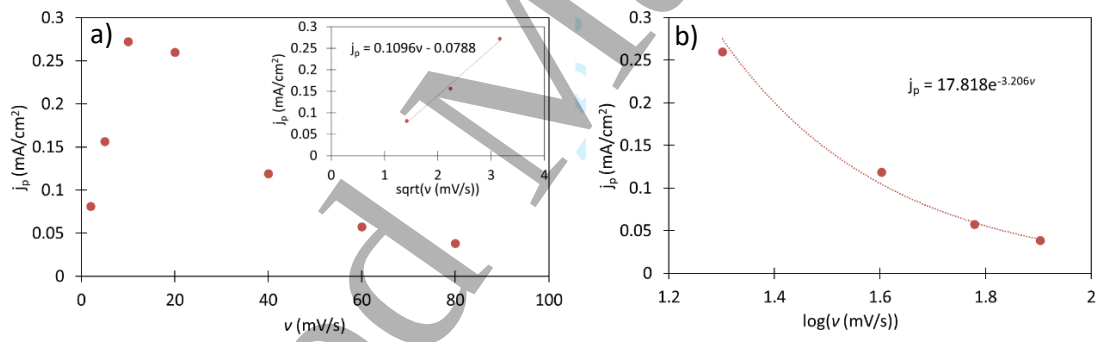

Figure 3. Peak current density (j_p) vs scan rate (v) showing a diffusion-controlled mechanism at lower scan rates and a kinetic controlled mechanism at higher scan rates. Suggesting that the Ga-LiOAc system is diffusion and kinetic controlled.

A galvanostatic charging test conducted by Perkins (1979) (28) showed a diffusion-controlled process in a similar potential window. In his work, an *i-t* plot from the galvanostatic charging test displayed a slope characteristic similar to a diffusion-controlled process ($it^{1/2}$), further suggesting that the oxidation region is diffusion controlled.

However, at higher v values, the exponential decrease of j_P with the v, suggests a kinetic controlled process where the electron transfer process is followed by a catalytic reaction. The mechanism as suggested by by Nicholson and Shain (31) can follow either a catalytic reaction with reversible charge transfer shown in Equations 7-8.

$$O + ne \rightleftharpoons R \quad (7)$$

$$R + Z \xrightarrow{k'f} O \qquad (8)$$

or catalytic reaction with irreversible charge transfer shown in Equations 9-10.

$$O + ne \xrightarrow{k} R \qquad (9)$$

$$R + Z \xrightarrow{k'f} O \qquad (10)$$

The first mechanism involves an irreversible catalytic reaction similar to that proposed by Perkins (1972) in Equation 2(29). This reaction is preceded by a reversible reaction. In both mechanisms, the catalytic reaction could be attributed to the disproportionation of electrochemically formed Ga_2O. The possibility of both reaction mechanisms occurring separately or simultaneously lies in the stability and instability of Ga surface oxides. Consequently, at higher scan rates the disproportionation reaction is the rate limiting step. This affects the amount of Ga_2O_3 accumulated, therefore, the magnitude of the reduction peak C_1 decreases.

Cyclic voltammetry of supporting electrolyte with Pr

Following the CV assessment of Ga in the supporting electrolyte, PrOAc was introduced into the electrolyte. Figure 4a shows a reduction peak (approximately -1.2 V), C_1, with a featured current density one magnitude greater (Insert Figure 4b) than the reported for peak C_1 in the absence of Pr (Figure 2). During the backward scan, the peak corresponding to hydrogen desorption (peak A* in Figure 2) is not observed. Subsequent cycles in the same scan range show a gradual decrease in the current density of peak C_1. When E_a is kept below -0.4 V, the current density of C_1 decreases, and eventually C_1 disappears as shown in Figure 4a.

Figure 4b shows that as E_a was increased above -0.4 V, C_1 reappeared and increased in current density. This suggests that Ga oxides may be key to the formation of Pr-Ga products observed in bulk electrolysis experiments presented below. Also, a nucleation loop (current on return sweep exceeding that of the forward sweep) was observed when more positive E_a values were applied. The appearance of the nucleation loop suggests the presence of an oxide layer whose thickness prevents the diffusion of Ga species. When this occurs, rather than diffusing through the oxide layer, metallic Ga likely accumulates on the surface of the oxide layer, acting as an extension to the surface area. Monnens et al. also observed this phenomenon while investigating the electrochemical behavior and deposition of Ga in 1,2-dimethoxyethane (DME) electrolytes(16).

Concentration of Pr vs current density

CV tests were performed with Pr concentrations from 15 mM to 50 mM to verify that the increase in current density of peak C_1 is directly associated to the presence of Pr. The insert in Figure 4a shows a linear relationship between the charge density of peak C_1 and the concentration of Pr, confirming that the increase in current density is due of the presence of Pr in solution and likely associated to Pr reduction.

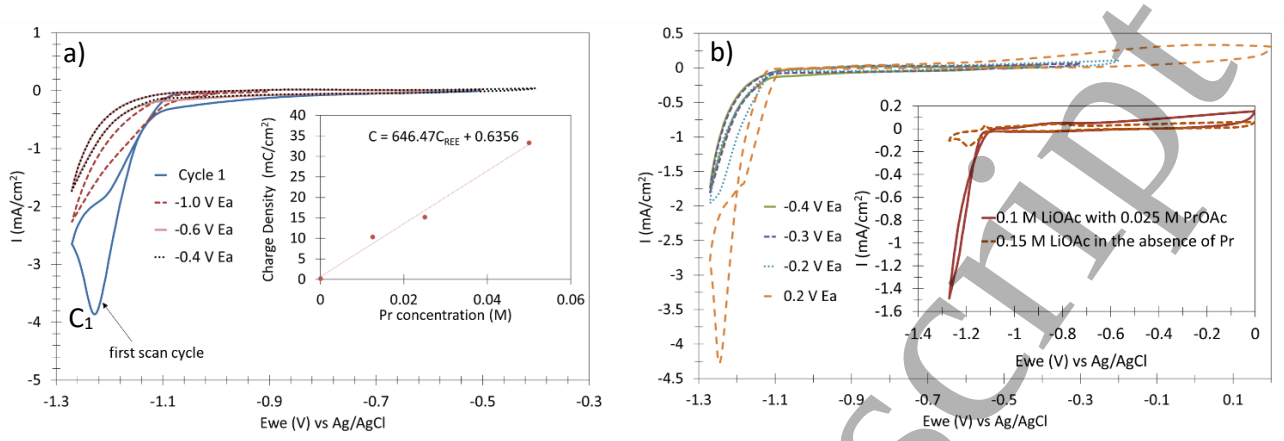

Figure 4. CV plots of Ga cathode at 10 mV/s a) in the presence of Pr with E_a -0.4 V (black dotted curve), -0.6V (solid pink curve), -1V (red dashed curve) with insert showing peak current for C_1 as a function of Pr concentration and b) in the presence of Pr with E_a above -0.4 V with insert comparing CV curves with (red curve) and without Pr (dark orange dashed curve).

Cyclic voltammetry scan rate study in the presence of Pr

A scan rate analysis was also performed after introducing Pr into the background electrolyte. Figure S5 illustrates CVs used to determine j_P as a function of v, where E_a was maintained at 0.2 V. These curves were analyzed to produce the data in Figure 5. The inset for Figure 5a shows that in the presence of Pr a linear relationship of j_p with v and $v^{1/2}$ is observed, suggesting a diffusion-controlled mechanism up to 10 mV/s. At higher scan rates an exponential decrease of j_P with v suggests a kinetically controlled process.

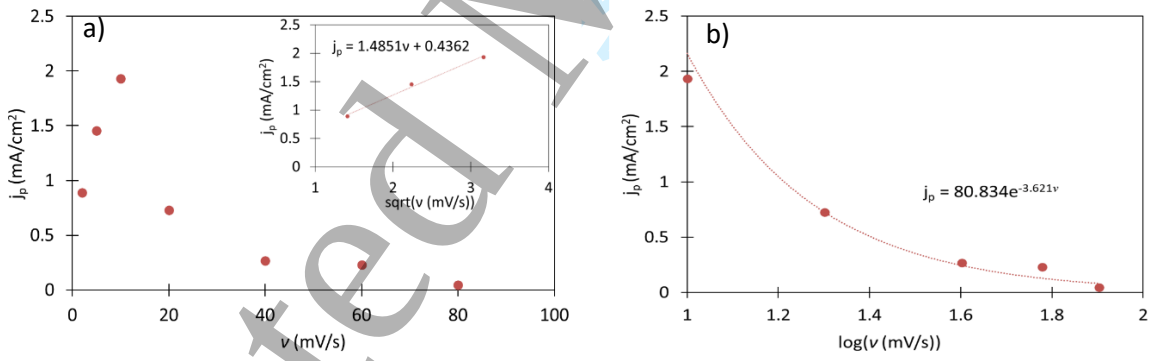

Figure 5. Peak current density vs scan rate showing a diffusion-controlled mechanism at lower scan rates and a kinetic controlled mechanism at high scan rates in the presence of Pr.

To this point is not clear what the effect of Pr is on the increase of cathodic current C_1. However, the kinetic analysis suggest that the reduction feature may involve a catalytic step as described in Equations 8 and 10. Further suggesting that Pr enhances Ga oxide formation possibly via chemical oxidation, prompting further studies.

Dark striations were observed on the surface of Ga as E_a approached more positive values in the presence of Pr. However, these striations disappeared as the sweep potential approached more negative values. These observations prompted a series of bulk electrolysis experiments designed to produce products for analysis.

Bulk electrolysis without flowing Ga cathode

Bulk electrolysis on a quiescent liquid Ga cathode was conducted in Pr containing electrolytes to investigate formation of Pr-Ga products. Chronoamperometric tests were carried out at potentials positive (-1.0 V) and negative (-1.3 V and -1.5 V) of the C_1 reduction feature. Tests at -1.0 V showed no visible qualitative changes on the surface of the Ga electrode throughout the duration of the experiment. At potentials of -1.3 V and -1.5 V, the formation of a light green precipitate was observed on the surface of the Ga as shown in Figure S6 shortly after the Ga surface transitioned from a dull to shinny look. ICP-MS analysis of the catholyte after electrolysis, illustrated in Figure 6, shows that the percentage of Pr removed from the catholyte increased (from 13% at -1.0 V, to 21% at -1.3V, and 35% at -1.5 V) as the potential was shifted to more negative values.

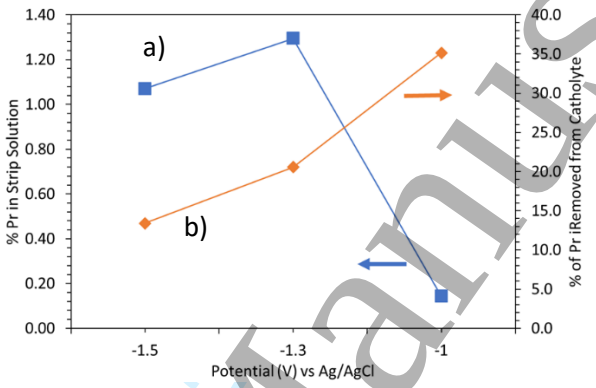

Figure 6. a) Blue line (□) represents the percentage of Pr in the leachate after stripping the liquid Ga in 1 M HCl. b) Orange plot (◊) shows the % of Pr removed from the catholyte during the electrolysis.

Following electrolysis, the liquid Ga was washed with DI water and digested in 1 M HCl to investigate the amount of Pr reduced into the surface of the Ga electrode. ICP-MS results of the digest showed that the amount of Pr captured into the Ga was only 0.1% at -1.0 V, 1.3% at -1.3 V and 1.1% at -1.5 V. These minuscule values do not agree with the loss of Pr removed from the catholyte illustrated in Figure 6. From Figure 2, it is seen that potentials below -1.2 V fall in the HER region. In this region, the formation of the light green precipitate can be explained as the precipitation of $Pr(OH)_3$ which follows Equations 11-12.

$$6H_2O \rightarrow 6OH^- + 3H_2 \quad (11)$$

$$2Pr^{3+} + 6OH^- \rightarrow 2Pr(OH)_3 \quad (12)$$

The ICP-MS analysis strongly suggests that the decrease in Pr concentration in the catholyte can be largely attributed to the formation of $Pr(OH)_3$. This analysis also suggests that even at potentials such as -1.0 V where the Ga is not being reduced, the removal of Pr via some other reaction path can be facilitated. XRD analysis of the green precipitate showed a highly amorphous material with a weak match for $Pr(OH)_3$ as seen in Figure S7. However, hydroxide rather than acetate is a more feasible product considering that acetate complexes are weaker. The results of the BE experiments suggest that bulk Pr reduction without stirring of the Ga surface does not take place at potentials below -1.2 V. Furthermore, these results do not provide insight about the increase in current density observed for reduction peak C_1 with Pr present. A key component absent from the initial BE experiments was the presence of Ga oxide which seem to play a significant role in the magnitude of the featured cathodic current.

Bulk electrolysis with flowing Ga cathode

Chemical oxidation of Ga was promoted via an external circulation loop where Ga was released drop by drop in the catholyte as a modification to the previous BE experiments. Dropping Ga through the catholyte into the pool allowed the formation of Ga oxides through chemical reaction when outside the pool (Figure 1b). Figure 7a shows the formation of a gray precipitate in the presence of Pr, which started forming even before any potential was applied. This occurs because the OCP of the Ga in this system is more positive than -0.9 V and lies in the region of Ga oxide formation. This gray precipitate was not observed when Ga was recirculated in LiOAc electrolyte in the absence of Pr, or in DI water. The formation of the gray precipitate, even in the absence of applied potential, was the first experimental suggestion that a disproportionation reaction involving Ga^{+} and Pr^{3+} may be play a role in the formation of a Pr-Ga product.

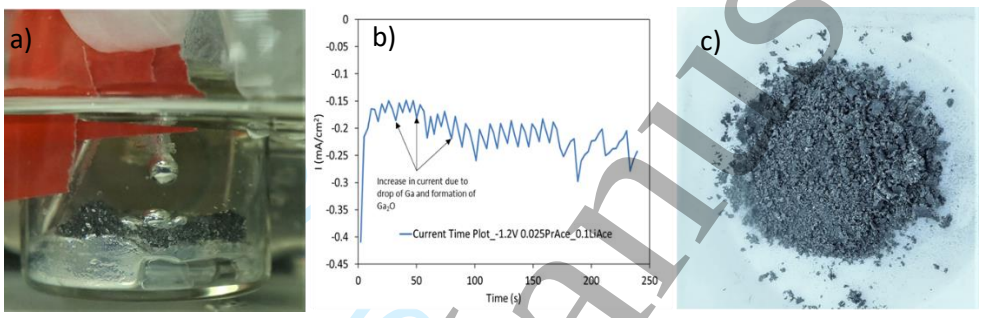

Figure 7. BE experiment at -1.2 V vs Ag/AgCl. a) Dropping of liquid Ga with gray precipitate formed in the presence of 0.05 M PrOAc and 0.1 LiOAc electrolyte at 30 °C, b) current vs. time curves while dropping Ga into the pool, and c) gray precipitate from electrolyte after BE after drying at 80 °C.

Understanding the effects of potential on the gray precipitate formation and its correlation to Pr, prompted separate 20-hr experiments with Ga recirculation at different potential scenarios. BE experiments were performed at OCP, -1.2 V and -1.3 V in an electrolyte containing LiOAc and PrOAc. For all these conditions, the gray precipitate was produced as Ga was circulated. When -1.2 V was applied to the system, an average current density increase of -0.246 mA/cm^2 was observed as Ga drops fell into the liquid Ga cathode as shown in Figure 7b. When filtered from the catholyte, and analyzed, the gray precipitate shown in Figure 7c contained >50% of the Pr initially present in the catholyte. The gray precipitate formed a distinctive solid phase that facilitated its separation from the liquid Ga. Digestion of the gray precipitate in 1 M HCl leaves a residue of Ga metal as shown in Figure S8e. During HCl digestion H_2 gas formation was observed, suggesting that the gray precipitate could have contained some Pr in the reduced state. While the gray precipitate remained solid after drying at 80 °C, the residual Ga from digestion of the gray precipitate in HCl melted at temperatures close to 30 °C as its original state. The phase diagram of the Pr-Ga system shown in Figure S9 suggests that a phase transformation from liquid gallium to solid product can be promoted by minimum additions of Pr. For example, the addition of as little as 1% Pr could result in the formation of an alloy with a melting point close to 200 °C. However, the formation of the gray precipitate does not prove that an alloy has been formed, or that Pr is being reduced. Rather it suggests the presence of some chemical reaction involving the Ga oxide and Pr where a different phase was formed.

The application of a suitable reducing potential is needed to facilitate the removal of Pr in significant amounts from the catholyte. Table 1 shows that for a solution with 50 mM PrOAc, the amount of Pr removed from the catholyte, and captured in the gray precipitate, with and without potential

application was 53.9% and 1.6 %, respectively. In the absence of applied potential, the formation of precipitate occurs but is limited by the formation of the unstable Ga_2O intermediate. Applied potential promotes the reduction of Ga(III) favoring continuous regeneration of Ga(I) and therefore co-disproportionation as hypothesized in Equations 13-15, which in the presence of Pr enhances the formation of the Pr-Ga product according to the Equations 17 and 18.

$$3Ga_2O_3 + 12H^+ + 12e^- \rightarrow 3Ga_2O + 6H_2O \quad (13)$$

$$3Ga_2O + Pr^{3+} \rightarrow Ga_3Pr + 3GaO^+ \quad (14)$$

$$2GaO^+ + H_2O = Ga_2O_3 + 2H^+ \quad (15)$$

Table 1. Percentage of Pr captured in the gray precipitate from the electrolyte.

Catholyte Composition	Potential (V)	Charge (C)	Time Run (hr)	Initial pH	Final pH	%Pr captured in precipitate
25 mM PrOAc	-1.3	180	20.0	6.5	11.0	83.3
25 mM PrOAc	-1.2	88	20.0	6.9	9.6	69.2
50 mM PrOAc	-1.2	122	20.0	6.5	7.8	53.9
50 mM PrOAc	No Potential	0	20.0	7.2	6.9	1.6

Higher Pr removals from the electrolyte, up to 83%, were obtained at -1.3 V. However, the characteristics of the product formed at -1.3 V are like those obtained during the bulk electrolysis experiments without agitation. This suggests a different mechanism, which could include the formation of $Pr(OH)_3$ influenced by high local pH at the cathode surface promoted by HER as discussed above.

Characterization of the precipitate

SEM and EDS were employed to determine morphology and composition of the gray precipitate. Figures 8 and S10a, and S10b are SEM images of the gray precipitate obtained at -1.2 V and -1.3 V, respectively. While both experiments were performed for the same length of time and in the same atmospheric conditions, a change in potential influenced the precipitate surface morphology. Comparisons between the precipitates for -1.2 V and -1.3 V suggests a coarser and aggregated texture at -1.2 V and a smoother texture at -1.3 V. EDS analysis of the precipitate obtained at -1.3 V shows a higher oxygen content than that obtained at -1.2 V as shown in Figure S10. Furthermore, EDS analysis of the precipitate obtained at -1.2 V (Figure 8a) show the presence of both Pr and oxygen in the precipitate. Close observation of Figure 8b, shows a spatial agreement between areas of high O and Pr, suggesting Pr oxides formed. A tentative explanation for this phenomenon could be that though the Pr can be reduced in the liquid Ga electrode, the product might not be stable in aqueous solution and undergoes rapid oxidation by reaction with water, leading to the formation of oxides.

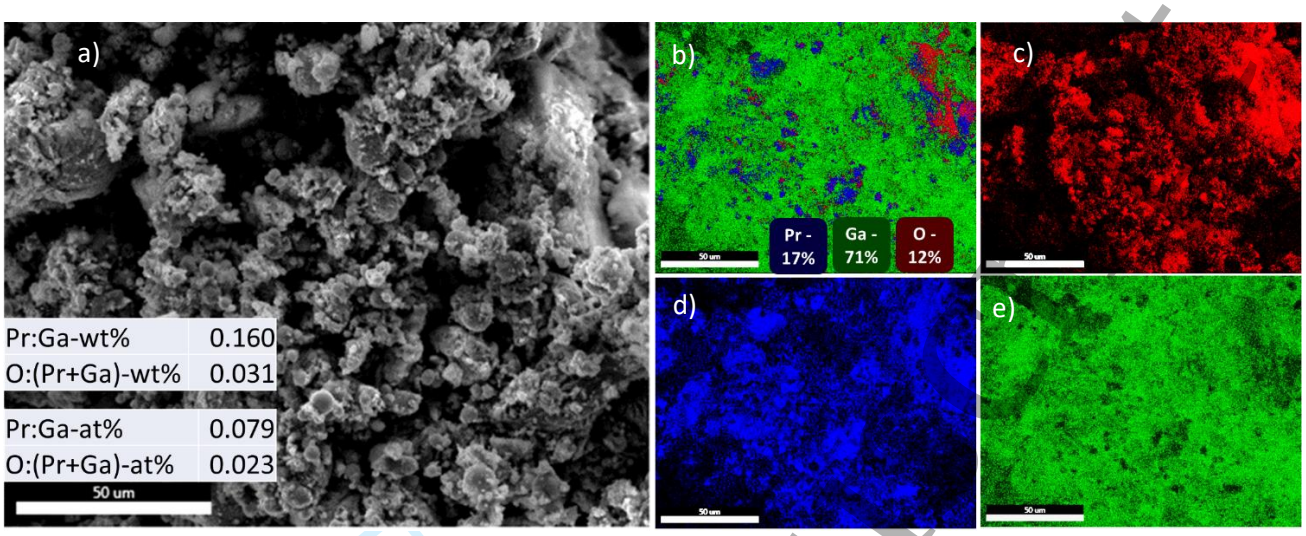

Figure 8. a) SEM imagery of gray precipitate at -1.2 V. b) EDS mapping showing Ga, Pr and O distribution at x100 at -1.2 V, c) red color O, d) blue color Pr, and e) Green color Ga.

These observations from the EDS analysis prompted further XRD analysis. Figure S11 shows that Ga metal is the only crystalline phase that can be identified from the product obtained at -1.2 V. The absence of identifiable Pr species suggests that no Pr metal or Ga-Pr alloys exist as a crystalline structure in the powder. This agrees with observations in Figure 8b. Further analysis of the overall oxygen content revealed an average value of 38 wt% O.

Analysis of the gray precipitate by Raman spectrum as seen in Figure 9 shows the presence of Ga_2O_3 and Pr_2O_3 peaks with comparable values to Wang (32), Zarembowitch (33), and Gouteron (34). A combination of Ga_2O_2 and Pr_2O_3 can be seen at 414.60 cm^{-1} and at 163.34 cm^{-1}. A closer observation of the Raman spectrum shows that the precipitate is compose mainly of Ga oxides. Additional characterization can be found in the accompanying supplementary document.

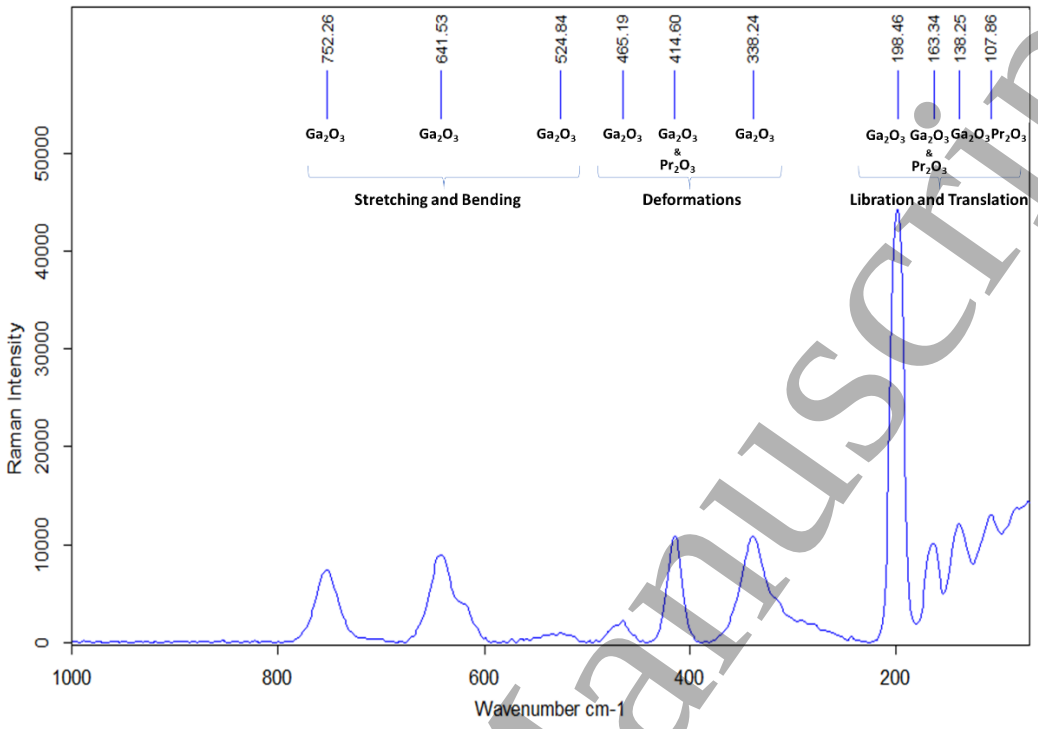

Figure 9. Raman spectrum of dark gray precipitate.

Conclusion

An alternate path to REE processing was investigated using liquid Ga as a cathode material. The reduction of Ga oxides in the presence of Pr showed an order of magnitude increase, when compared to in the absence of Pr, accompanied by the formation of a solid powder phase rich in Pr. Window opening CV and scan rate analysis established that Ga reduction follows a kinetic controlled mechanism where a catalytic reaction follows an electron transfer. This mechanism was then explained by means of Ga disproportionation, which is enhanced by the presence of Pr. Therefore, Pr enhanced disproportionation led to the formation of an additional solid phase (gray precipitate) during BE where > 50% of the Pr can be concentrated from diluted aqueous electrolytes. The formation of this gray precipitate only occurred when Ga was circulated and introduced back into the Ga pool via a pump. Circulation of the liquid Ga enabled the formation of surface oxides which are crucial for the formation of the gray precipitate. Furthermore, digestion of this precipitate in 1 M HCl produced H_2 gas and returns Ga to its original state. The above process discussed proves the feasibility of recovering REEs in a solid concentrate using liquid Ga cathode redox chemistry as capture mechanism.

Acknowledgement

This manuscript has been authored by Battelle Energy Alliance, LLC under Contract No. DE-AC07-05ID14517 with the U.S. Department of Energy. This study was supported by funding provided by the Critical Materials Institute, an Energy Innovation Hub funded by the U.S. Department of Energy, Office of Energy Efficiency and Renewable Energy, Advanced Manufacturing Office. The authors wish to also express their sincere thanks to Byron White, Tim Yoder, Dr. Lorenzo Vega Montoto and Kunal Mondal from Idaho National Laboratory, and Andre Anderko from Oli System for offering their support and expertise during this project.

References

1. A. P. Abbott and K. J. McKenzie, *Physical Chemistry Chemical Physics*, **8**, 4265 (2006).
2. S. Venkatesh and B. V. Tilak, *Journal of Chemical Education*, **60**, 276 (1983).
3. J. Crook and A. Mousavi, *Environmental Forensics*, **17**, 211 (2016).
4. E. I. Onstott, *Journal of the American Chemical Society*, **78**, 2070 (1956).
5. G. M. Kolesov and L. N. Pankratova, *Russian Chemical Reviews*, **37**, 701 (1968).
6. Ø. Mikkelsen and K. H. Schrøder, *Electroanalysis*, **15**, 679 (2003).
7. V. P. Shvedov and P. G. antonov, *Radiokhimiya*, **5**, 342 (1963).
8. E. Onstott, *Analytical Chemistry*, **33**, 1470 (1961).
9. L. Airey, *The Analyst*, **72**, 304 (1947).
10. N. J. Langford and R. E. Ferner, *Journal of Human Hypertension*, **13**, 651 (1999).
11. P. Surmann and H. Zeyat, *Analytical and Bioanalytical Chemistry*, **383**, 1009 (2005).
12. Y. Chung and C.-W. Lee, *J. Electrochem. Sci. Technol*, **4**, 1 (2013).
13. D. Belaschk, *Zeitschrift für Physikalische Chemie*, **234**, 258 (1967).
14. M. Pourbaix, *Atlas of electrochemical equilibria in aqueous solution* (1974).
15. D. O. Flamini, S. B. Saidman and J. B. Bessone, *Journal of Applied Electrochemistry*, **37**, 467 (2007).
16. W. Monnens, P.-C. Lin, C. Deferm, K. Binnemans and J. Fransaer, *Physical Chemistry Chemical Physics*, **23**, 15492 (2021).
17. B. Hong, Y. Wang, X. Wei, Q. Huang, X. Wang, T. Fujita and Y. Wei, *Hydrometallurgy*, **194**, 105344 (2020).
18. C. J. Powell, *Physical Review*, **175**, 972 (1968).
19. J.-E. Park, H. S. Kang, J. Baek, T. H. Park, S. Oh, H. Lee, M. Koo and C. Park, *ACS Nano*, **13**, 9122 (2019).
20. D. Wang, C. Gao, W. Wang, M. Sun, B. Guo, H. Xie and Q. He, *ACS Nano*, **12**, 10212 (2018).
21. M. Mayyas, M. Mousavi, M. B. Ghasemian, R. Abbasi, H. Li, M. J. Christoe, J. Han, Y. Wang, C. Zhang, M. A. Rahim, J. Tang, J. Yang, D. Esrafilzadeh, R. Jalili, F.-M. Allioux, A. P. O'Mullane and K. Kalantar-Zadeh, *ACS Nano*, **14**, 14070 (2020).
22. J. Han, M. Mayyas, J. Tang, M. Mousavi, S. A. Idrus-Saidi, S. Cai, Z. Cao, Y. Wang, J. Tang, R. Jalili, A. P. O'Mullane, R. B. Kaner, K. Khoshmanesh and K. Kalantar-Zadeh, *Matter*, **4**, 4022 (2021).
23. M. B. Ghasemian, M. Mayyas, S. A. Idrus-Saidi, M. A. Jamal, J. Yang, S. S. Mofarah, E. Adabifiroozjaei, J. Tang, N. Syed, A. P. O'Mullane, T. Daeneke and K. Kalantar-Zadeh, *Advanced Functional Materials*, **29**, 1901649 (2019).
24. B. Lertanantawong, P. Lertsathitphong and A. P. O'Mullane, *Electrochemistry Communications*, **93**, 15 (2018).
25. Y. Wang, S. Wang, H. Chang and W. Rao, *Advanced Materials Interfaces*, **7**, 2000626 (2020).
26. A. Varadharaj and G. P. Rao, *Proceedings of the Indian Academy of Sciences - Chemical Sciences*, **102**, 177 (1990).
27. A. Tsvetanova, E. Sokolova and S. Raicheva, MECHANISM OF ANODIC-DISSOLUTION OF GALLIUM IN ACIDIC AQUEOUS-SOLUTIONS, in, p. 185, PLENUM PUBL CORP CONSULTANTS BUREAU, 233 SPRING ST, NEW YORK, NY 10013 (1979).
28. R. S. Perkins, *Journal of Electroanalytical Chemistry and Interfacial Electrochemistry*, **101**, 47 (1979).
29. R. Perkins, *J Electrochem Soc*, **119**, 713 (1972).
30. M. A. Creighton, M. C. Yuen, M. A. Susner, Z. Farrell, B. Maruyama and C. E. Tabor, *Langmuir*, **36**, 12933 (2020).

31. R. S. Nicholson and I. Shain, *Analytical chemistry*, **36**, 706 (1964).
32. G. Wang, J. Park, X. Kong, P. R. Wilson, Z. Chen and J.-h. Ahn, *Crystal Growth & Design*, **8**, 1940 (2008).
33. J. Zarembowitch, J. Gouteron and A. M. Lejus, *physica status solidi (b)*, **94**, 249 (1979).
34. J. Gouteron, D. Michel, A. M. Lejus and J. Zarembowitch, *Journal of Solid State Chemistry*, **38**, 288 (1981).